



AirCargoChallenge 2022

Technical Report

Team #09

HERMES TEAM



Table of Contents

Table of Contents	2
1. Introduction	4
2. Project management (financial budget and time schedule)	5
3. Aerodynamic design	8
3.0.1. Design – Design Variables	8
3.0.2. Flight Performance Analysis	10
3.1 Aerodynamic Analysis	11
3.1.1. Panel Methods and XFLR5	11
3.1.2. Lifting Line Theory (LLT) and Open Vogel	11
3.1.3. Aircraft Lift and Drag prediction	12
3.2. Propeller Performance – Wind Tunnel Experiment	12
3.2.1. Wind tunnel experiment	13
3.3. Longitudinal Stability and Tail Sizing	13
3.4. Mission Performance Analysis	14
3.4.1. Calculating the SEP contours	15
3.5. Optimization	15
3.5.1. Genetic Algorithm	15
3.5.2. Methodology:	16
3.5.3. Constraint Handling in Optimization	16
3.5.4. Process of Design – Analysis and Optimization	17
4. Results validation via the use of Computational Fluid Dynamics	17
4.1. Basic Principles of Computational Fluid Mechanics	17
4.2. Basics of Fluid Engineering	17
4.2.1. Continuity Equation	18
4.2.2. Momentum Conservation Equation	18
4.2.3. Energy Conservation Equation	18

4.3. Finite Volume Method	18
4.3.1. 2-D Finite Volume Method	19
4.3.2. FVM Discretization Grid	20
4.4. Hermes V CFD Simulation	20
4.4.1. Turbulence Model	21
4.4.2. RANS Turbulence Models	21
4.4.3. Boussinesq Case	22
4.4.4. Spalart-Allmaras Turbulence Model	22
5. Structural design	24
5.1 Model Design	24
5.2 Structural analysis	25
5.2.1 Mesh	26
5.2.2. Case Setup	26
5.2.3. Simulation	26
6. Payload prediction	28
7. Manufacturing	29
7.1 Material Selection	29
7.2 Manufacturing Process	30
7.2.1 Type A Construction Process	30
7.2.2 Type B Construction Process	31
8. Telemetry Development	33
9. Outlook	36
10. Drawings	37

1. Introduction

The current report serves to demonstrate and explain the design and design philosophy of an Unmanned Aerial Vehicle (UAV) that was studied and is manufactured for the Air Cargo Challenge (ACC) competition held in Munich between July 5th and July 8th this year (2022).

The Hermes Team and all of its members were organized and managed under the auspices of EUROAVIA Athens which exists within the larger EUROAVIA organization.

EUROAVIA is the European Association of Aerospace Students. It's a volunteer, non-profit organization that consists of students interested in aerospace engineering and generally the field of mechanical engineering. It was established in 1959 and up to now counts more than 40 Affiliated Societies, in 20 countries of Europe for a total of more than 2000 members. One of these Affiliated Societies is EUROAVIA Athens.

EUROAVIA Athens first came together in early 2006, with the support of the National Technical University of Athens (NTUA). Our team members are aspiring engineers and students who are interested in aerospace. The desire for knowledge, as well as the interest in aerospace, has created a community of people eager to explore ideas and put them to the test. Among them exists the Hermes Team with the purpose of participating in the ACC competition, one of the cornerstone technical projects of our organization.

The Hermes Team has been subdivided in 4 subteams, namely: Aerodynamics, Structural, Manufacturing, and Electrical. Each group focuses on a specific part of the airplane design, while communicating with each other closely. The whole project is overseen by the team leader who is responsible for steering the team and facilitating communication and cooperation.

The Covid-19 pandemic presented a new reality in which our team had to adjust. Unfortunately the 2021 ACC got postponed. We took the opportunity in this and worked even harder to compete this summer in Munich with the best possible aircraft we could manufacture. As a team we had to tackle the leaving of many members and recruit new ones to cover their absence.

The task of the newly updated ACC also intrigued our team with its realistic mission of transporting blood bags with unmanned aerial vehicles. Every year, our country faces many natural disasters, such as floods and fires. This results in many villages being cut off and many lives put in jeopardy. So, research and experience in this area of interest could be a starting point to develop the needed infrastructure to support these crisis scenarios.

Working closely as a team with many brainstorming sessions we decided to start with a clean slate for this competition. We worked on taking an innovative approach for the design that we believe will differentiate us and give us an edge.

2. Project management (financial budget and time schedule)

The Hermes Team consists of members of EUROAVIA Athens that are recruited and interviewed regarding their knowledge in the design and manufacturing of airplanes and their passion towards this field of engineering. Most of the members are from the school of Mechanical Engineering of the National Technical University of Athens, the leading polytechnic school of Greece.

The Air Cargo Challenge competition has presented a specific challenge for our organization in the years we have participated. Specifically, for a team to excel in the competition a high level of understanding and expertise in aerodynamics and structural analysis and modeling is required. In our university, such courses are explored in the latter years of the Integrated Masters curriculum. Therefore, students with the prerequisite knowledge to get involved in such a project are mostly in their 4th or 5th years of studying and typically finish their studies at the same time the competition takes place and thus leave the team.

This problem is stifling team knowledge continuity as each participating team has to start over with little guidance. One of the primary goals behind the structuring of the new Hermes V team was to change that. After much consideration, it was deemed optimal to discard previous iterations of the Hermes Team designs and start with a clean slate. We also made the decision to expand our team so that more of the members of EUROAVIA Athens can get exposed to the technical aspect of aerospace engineering with hands-on experience, even though at many times they could not contribute significantly.

The Hermes Team was initially formed in 2020 with the goal of participating in the 2021 competition. Most of the active members were in their 4th or 5th years of studying,, with orientations that vary from control systems and manufacturing to computational fluid dynamics (CFD) and aerodynamics. Among them, it was decided to include younger members as trainees.

During the pandemic and especially during the lockdowns, the ability of our team to collaborate efficiently was severely affected. Although we quickly adapted to remote work, through various voice and video meetings, we found many obstacles regarding the cooperation with outside parties that stifled our performance.

After the postponement of the competition, most of the core members of the team had to leave, as they were done with their degree. The positions they left, however, were quickly filled and we continued working eagerly.

At the moment the team consists of 15 members and 5 trainees, as can be seen in the table below.

Name	Position	Qualifications
Spyridon Voutsinas	Professor in Charge	Mechanical Engineering Professor, PhD with interest in CFD

#09 Hermes Team | EUROAVIA Athens | Technical Report ACC 2022

Christos Papachristodoulou	Team Leader	4th year, Mechanical Engineering, with expertise in Aerospace
Tryfonas Themias	Team Member President of EUROAVIA Athens	4th year, Mechanical Engineering, with expertise in Aerospace
Giorgos Lazarou	Aerodynamics Team Leader	Masters in Aerospace Engineering
Vasilis Faliakos	Structural Design Leader	4th year, Mechanical Engineering, with expertise in Aerospace
Andreas Mitakidis	Electrical Team Leader	5th year, Electrical Engineering,
Vasilis Dellas	Manufacturing Team Leader	5th year, Mechanical Engineering, with expertise in Energy
Titos Dellis	Aerodynamics	4th year, Mechanical Engineering, with expertise in Aerospace
Nikolas Theodorou	Aerodynamics	4th year, Mechanical Engineering, with expertise in Energy
Giannis Skoulikas	Aerodynamics	2nd year, Mechanical Engineering
Ilias Mitropapas	Aerodynamics	3d year, Mechanical Engineering
Athina Pantazi	Manufacturing	4th year, Mechanical Engineering, with expertise in Constructions
Panagiotis Bounas	Manufacturing	3d year, Mechanical Engineering
Michalis Karallis	Aerodynamics	Masters in CFD
Alexis Vavas	Electrical	2nd year, Mechanical Engineering
Sofia Georgopoulou	Trainee	2nd year, Mechanical Engineering
Giorgos Papamichail	Trainee	2nd year, Mechanical Engineering
Dimitris Mantogiannis	Trainee	2nd year, Mechanical Engineering
Georgios Chatzigiannis	Trainee	4th year, Mechanical Engineering, with expertise in Aerospace

Athina Maria Athanassaki	Trainee	1st year, Mechanical Engineering
Andreas Kanteres	Trainee	3d year, Mechanical Engineering

Members that left after the postponement of the competition are also mentioned in the table below with their qualifications as of the time of their departure.

Name	Position	Qualifications
Giorgos Smyrlis	Former Team Leader	Mechanical Engineer, with expertise in Aerospace
John Baklagis	Aerodynamics	Mechanical Engineer, with expertise in Aerospace
Michalis Skiadopoulos	Structural	Mechanical Engineer, with expertise in Construction
Panagiotis Koronaios	Structural	Mechanical Engineer, with expertise in Construction
Dimitris Dimos	Aerodynamics	Mechanical Engineer, with expertise in Aerospace

The Hermes Team operated in 4 main subgroups that, although independent, typically discussed decisions and ideas among them. The Aerodynamics subgroup decided and optimized the design of all aerodynamic surfaces with the goal of maximizing the performance in accordance with the competition scoring. The Structural Design subgroup created the 3D CAD models for the airplane to suit all the practical requirements (Cargo Bay, Motor Base etc.) examining their structural integrity using Finite Element Analysis and finally choosing suitable materials. The Electrical subgroup designed and implemented a newly developed telemetry system and flight data analysis system along with the aircraft's electrical systems. Finally, the Manufacturing subgroup was responsible for researching material properties and manufacturing methods, testing the feasibility of prospective design ideas, and finally materializing each specific part of the airplane.

The full design of the aircraft was finalized in April 2022, after the combination of the results and conclusions of the aforementioned subgroups.

The total budget used for the construction of the aircraft, with some additional/spare parts, is right now around 3075€ and we are expecting another 500€ in manufacturing expenses . The

budget for the participation of the 7 members (6 team members, 1 pilot) is 1750€ and for the transportation is expected to be around 1750€. For the remaining team members that may follow the team as guests the cost is difficult to be determined yet.

3. Aerodynamic design

3.0.1. Design – Design Variables

The main objective for the aerodynamic design of HERMES V was the aircraft's optimal performance in the ACC. The function that evaluates such performance given by the ACC rules is the following:

$$S = \left(\frac{S_{height}}{S_{height,best}} + \frac{S_{dist}}{S_{dist,best}} + \frac{S_{payload}}{S_{payload,best}} \right) \cdot B_{take-off},$$

which gives the relation between the total points scored during flight and the height, distance and payload transportation achieved. The score for each of those variables (height,distance,payload) is calculated by dividing the UAV's performance by the best score achieved in each segment in the competition. The sum of these values are then multiplied by the take-off factor, which is equal to 1.1 if take-off distance is less than 40 meters. It must be noted that here only the points related to the flight performance are examined. Loading, unloading and payload prediction are not taken into consideration yet.

The ACC approach for evaluating contestants motivated the team to examine different designs for the HERMES V. Thus, it was decided to define the most important factors for flight performance as independent design variables. The combination of Genetic Algorithm (GA) and Aircraft Analysis was implemented in order to model the competition between different designs and determine the optimal combination of the design variables. As mentioned above, these variables were chosen after considering the most important factors for the aircraft's flight performance and are related to the design of the main wing and fuselage.

The design variables were:

- Root chord (meters) : The chord length of the airfoil at the root of the wing
- Tip chord (meters) : The chord length of the airfoil at the tip of the wing
- Airfoil (given 2D shape) : After research, 11 airfoils were chosen to be analyzed and compared for the design of the main wing. The airfoils were chosen to be:
 1. NACA 0008
 2. AG25
 3. CLARK Y
 4. GEMINI
 5. GOE 398
 6. GOE 533
 7. NACA 4415
 8. NACA 64(3)-618
 9. SD7032
 10. SG6043

11. TsAGI-R3A

For the empennage, airfoil NACA 0008 was used.

- Incidence Angle (degrees) : The angle between the root chord line and the longitudinal axis of the aircraft (fuselage)
- Fuselage length (meters) : the length of the aircraft's fuselage
- Payload (Newton) : The gravitational weight of the cargo mass (depends on the no. of blood bags)
- Semi- Span (meters) : The distance between the tip of the main wing and the axis of lateral symmetry (located in the fuselage)
- Wing longitudinal position (meters) : The distance between the main wing's leading edge and the aircraft's nose

It was also decided that the main wing will not have sweepback due to the fact that the flight's Mach numbers are too low (0.08-0.1) for compressible and transient phenomena and thus sweepback was considered irrelevant.

Furthermore, the analysis and optimization of HERMES V was carried out in accordance with the ACC constraints. This will be discussed thoroughly in the segment titled "Optimization".

Nomenclature:

Lift Coefficient (C_L): Dimensionless coefficient that relates Lift with Area and Dynamic Pressure, expression:

$$C_L = L / (0.5 * \rho * S * V^2)$$

where,

ρ = density (kg/m^2)

L = Lift (N)

V = Velocity (m/s)

S = associated reference area (m^2)

Drag Coefficient (C_D) and Moment Coefficient (C_M) are similarly defined dimensionless coefficients for a body's Drag and Pitching Moment

Reynolds Number: Dimensionless quantity that characterizes a fluid flow. Generally speaking, high numbers belong to turbulent flows while low indicate laminar flows.

Expression:

$$Re = V * l / \nu$$

where,

V = velocity,

L = characteristic length(m), e.g Chord length

ν = kinematic viscosity of a fluid i.e. viscosity divided by density (poise)

Mach number (**Ma**) : Dimensionless fluid speed, related to the speed of sound:

$$M = V * a$$

where,

α = speed of sound

3.0.2. Flight Performance Analysis

In order to evaluate a given combination of the 8 design variables the following were applied.

- Aerodynamic Analysis: Determining the Aircraft's Lift and Drag Coefficient in different angles of attack and Reynolds numbers.
- Propeller Performance Analysis: Determining the model for engine operation under different airspeeds.
- Static Stability Analysis: Ensuring the aircraft's static lateral stability and determining the static margin.
- Mission Performance Analysis : Calculating the optimal combination of Mach number and Height during flight, in order to determine the best possible score that the given design can achieve. Furthermore, this height- Mach curve will assist the team's pilot during flight testing.

3.1 Aerodynamic Analysis

The goal for the UAV's aerodynamic analysis was the determination of the Lift Coefficient – Drag Coefficient for a certain range of Reynolds numbers. These CL-CD functions will be crucial for the flight performance modeling which is described later.

The team relied on inviscid models whose calculations require little time and computational cost. The two methods that are implemented are the panel methods and lifting line theory.

3.1.1. Panel Methods and XFLR5

Panel Methods rely on Potential Flow Theory. After assuming that the flow is irrotational, incompressible and that the fluid is inviscid, the lifting surface's geometry is discretized. In each geometric segment the no-penetration condition must be satisfied. The no-penetration condition is a boundary condition for inviscid flows and it states that in the presence of a solid body, the fluid's velocity relative to the one of the solid wall must be equal to zero in the direction normal to the wall. For example if we assume a stationary object, the normal component of the flow velocity near the walls will be 0.

A series of potential flow singularities such as sources and doublets are used to model the flow in each panel and the body's wake. The values of these singularities are calculated via the satisfaction of the boundary condition and then the velocity field is known. Then, the pressure distribution (the inviscid, incompressible assumption permits the use of the bernoulli equation) and Lift Coefficient can be obtained. However no useful information in terms of Drag can be acquired from such methods.

However, the software used to apply the 2D panel method in the 10 airfoils for our concern , the free to use XFLR5, uses the XFOIL code, which is capable of solving inviscid and boundary layer equations simultaneously. This method was developed in the 1990s by M. Dreal and H. Youngren. Therefore, the airfoils of our concern were analyzed in different angles of attack and Reynolds numbers and Drag and Lift polars, that would be used later in the analysis and optimization were acquired.

3.1.2. Lifting Line Theory (LLT) and Open Vogel

With LLT the aerodynamic forces can be calculated in a 3D case. In an aerodynamic surface with finite span, whose 2D aerodynamic forces are known, the circulation of downwash velocities and vorticity in the span-wise direction can be obtained. Thus the 3D Lift and induced Drag due to wing tip vortices can be calculated.

This was applied via the open-source program Open Vogel. For a given design the 2D information is used in order to calculate the 3D aerodynamic forces. The positions and dimensions of each lifting surface, along with their 2D Lift and Drag polars are sufficient input for the software to determine the 3D Lift and and Drag at a given angle of attack.

3.1.3. Aircraft Lift and Drag prediction

The goal of the aerodynamic analysis of an aircraft design is gaining information for its lift and Drag at different angles of attack, via lift and drag polars. This will later be used in the aircraft's flight performance analysis. Having determined an aircraft's 3D aerodynamic forces at a given angle of attack, the team made use of the following formula, which correlates the Drag Coefficient with the Lift Coefficient:

$$C_D = C_{do} + C_l^2 / (\pi * AR * e)$$

where,

CD is the Drag coefficient,

CL is the lift coefficient, the first term of the equation is the Drag coefficient at zero angle of attack (due to pressure distribution , shear stresses) ,the second term is the Lift induced Drag, **AR** is the aspect ratio and e is an efficiency factor whose value is below zero (1 is for an elliptical body).

For a given geometry, it is possible to determine 3D aerodynamic forces for angles of attack between 0 and 10 degrees with an increment of 1 degree. This results in different pairs of CL and

CD which are then used as control points of curve-fitting in order to determine a CD(CL) function of the following form:

$$C_D = C_{do} + k * C_l^2$$

These aerodynamic calculations can occasionally fail to converge and calculate results for a given angle of attack. The team decided that there should be at least five converged points for the curve fitting to take place. In any other case the design would be discarded. This decision was crucial for bound optimization's computational cost and needed time for convergence.

These CD (CL) functions, each for different Reynolds number will be crucial for any aircraft's evaluation.

3.2. Propeller Performance – Wind Tunnel Experiment

Crucial for flight performance modeling is the presence of the Thrust – Velocity (T-V) diagram of the aircraft's propeller engine. It was decided to take measurements in order to produce said diagram for both of the ACC provided propellers and choose one of them with this information. An experimental procedure was carried out in order to acquire thrust values for different velocities which would then be curve-fitted producing a T-V diagram. The experiments were carried out in full throttle conditions because the small duration of the ACC rounds render energy conservation during flight unnecessary.

3.2.1. Wind tunnel experiment

In order to define the thrust of the motor engine ,that is needed for the Energy Maneuverability Theory,we made an assembly consisted of;

- 2 different propeller
- the battery
- the engine
- speed controller
- pitot tube
- a breadboard and arduino
- load sensor

The team took measurements for both propellers (15 each) and for each one we had temperature and pressure known(0.005kPa-0.265kPa).

The line of the connection was propeller->engine->speed controller->battery->receiver. We had to be careful with the calibration of the arduino and with the orientation of the pitot tube.

So, during the different air speed flows , we measured the thrust of the engine. This was accomplished because the assembly had the load sensor(piezoelectric) which, through the arduino ,transformed the grams into Volts of each measurement. In the end, we had a realistic view of what our engine is capable of(diagrams of Thrust-air velocity) ,despite the constructor's

measures. The team also made tests to check the battery's c-rate when our engine is in full throttle.



3.3. Longitudinal Stability and Tail Sizing

Crucial for HERMES V was ensuring the UAV's static longitudinal stability. The condition that must be satisfied is that the center of mass must be located in front of the neutral point of the aircraft. Neutral point is the position on the longitudinal axis of the aircraft where the Moment Coefficient (CM) is independent of the angle of attack. If this condition is true, the aircraft's moment coefficient has a negative slope with respect to its angle of attack. Thus, at any moment, if the angle of attack suddenly changes, the aerodynamic forces will act in favor of the aircraft's return to its initial state. The distance of the center of gravity and neutral point as a percentage of the aircraft's mean aerodynamic chord is called static margin.

As it is discussed above, the tail of the aircraft was not considered a design variable. Thus, its geometrical characteristics were determined through the following process:

A case where the aircraft's center of gravity is located in the most rearward position is considered (30% MAC). In this case, it is examined if it is possible to add a stabilizer, sufficient enough for achieving stability, with a static margin equal to 10% MAC.

$$x_{cg@0.3MAC} = x_{NP} - 0.1 * MAC)$$

This process determines the dimensions for the stabilizer that provide the required stability margin. It is possible that there is no possible stabilizer design. In this case, this aircraft design is discarded.

3.4. Mission Performance Analysis

Energy Maneuverability Theory is a quantitative model of flight performance, developed by Col. John Boyd and Thomas P. Christie in 1966. The general idea is to evaluate an aircraft's performance based on its excess power, potential and kinetic energy. Through the examination of these variables the model can determine the optimal combination of Mach number and

Altitude (Alt-M) waypoints for different objectives, such as minimum time, minimum fuel consumption. This calculation is based on Routowski Paths, a method developed by E.S. Routowski. It is important to note that this theory relies on the assumption of small angles of attack and climb and steady state conditions.

The team's concern was to model any aircraft's performance in the minimum time climb conditions and extract its potential score in the ACC through that process.

Firstly, a Specific Energy Diagram is produced. This consists of a 2D diagram with Mach number in the x axis and altitude (m) in the y axis. Curves, called specific energy contours are drawn in which the following value is constant:

$$E_s = H + V^2/(2 * g)$$

where,

H is the altitude (m)

V is the velocity (m/s)

g is the gravitational acceleration (m/s²).

The Specific Excess Power contours (SEP) are then drawn. These are curves where the aircraft's specific excess power is constant. The specific excess power is given by the following expression:

$$SEP = (T - D)/W * V$$

where,

T is the thrust (N)

D is the Drag (N)

W is the gravitational weight of the aircraft (N).

These curves express the aircraft's ability to gain energy. According to Routowski, the points where the SEP contours are tangential to the Specific Energy contours express the optimal path that needs to be followed by the pilot in order to achieve the minimum time climb.

3.4.1. Calculating the SEP contours

While the drawing of the Specific Energy Contours is a fairly simple task, such is not true for the SEP contours. For a given design, each point in the Alt-M diagram is examined. The value of the Reynolds number (and thus the aerodynamic performance of the aircraft) depends on the Mach and altitude values.

The process for calculating SEP for each point in Alt-M diagram:

1. Thrust value for the given velocity is imported (T-V diagram)

2. Reynolds number is calculated
3. CL(CD) function for this Re is imported
4. Point in CL(CD), for which Lift = Weight is located. Lift and Drag are calculated. If the Lift = Weight condition cannot be satisfied, this point is not relevant to the Routwski path.
5. SEP is calculated

After this process the data is sufficient for the drawing of the SEP contours and the minimum time climb path, which provides the team with important information regarding a design's capabilities for gathering points at the ACC.

3.5. Optimization

As mentioned above, the HERMES V design was analyzed with the aforementioned methods and optimized through the implementation of a Genetic Algorithm.

3.5.1. Genetic Algorithm

A genetic algorithm is a very popular non-deterministic, population-based approach to optimization problems that belongs to the larger class of Evolutionary Algorithms. The term "Evolutionary" implies that these algorithms are inspired by Darwin's Natural Selection. There are many versions and approaches in the implementation of a Genetic Algorithm. The fundamental methodology, which was followed by the team is presented below.

3.5.2. Methodology:

The design variables are defined and parameterized and bounded. An objective function is also defined, also called fitness function. The goal is to find the design that either maximizes or minimizes said function. The user also decides a number of population members, crossover process, parent selection method and mutation factor.

1. A Random Number Generator (RNG) produces initial values for the design variables within the design space, for each member of the population i.e. a different design.
2. All the population members are evaluated, the objective function for each combination of the design variables is calculated. The population members are sorted with respect to the values of the objective function.
3. Parent selection occurs. The most popular method is called Roulette Wheel Selection. In this method, the population members are put in a roulette wheel and the space that each member occupies is proportional to its fitness. The wheel turns, deciding which pairs of members will be put through the crossover process. These members are named parents.
4. The parents are put through the crossover process, which gives a combination of the values of each parent for each design variable. The coding of the design variables plays an important role in this step. The team used real coding. A simple crossover method for design variables coded with real numbers is presented below for two genes X1, X2 from two individuals Y1, Y2:

$$\text{If } x_1 < x_2 \text{ then } x_{\text{offspring}} \in [x_1 - a * (x_2 - x_1), x_2 + a * (x_2 - x_1)]$$

5. New population members are created, but the best member(s) from the previous generation are maintained. The sum of these designs consist of the new generation.
6. A mutation factor can be introduced to increase search space exploration. This factor randomly mutates the genes of an individual with a probability equal to the selected factor.

Steps 2 through 5 are carried out for many generations until a termination condition is satisfied. It was decided that the GA of the UAV optimization will stop when convergence occurs. The optimization stops when the objective function of the fittest members does not change for a number of generations.

3.5.3. Constraint Handling in Optimization

It is vital for the final design of HERMES V to follow the ACC constraints. In order to satisfy this condition, the fitness score of population members whose designs were out of the spatial boundaries of the ACC constraints was penalized.

The GA was programmed to find the maximum of the S function, where S is the score function described above. Therefore, penalization is achieved through assigning a score regarding a design's divergence of the spatial limitations.

3.5.4. Process of Design – Analysis and Optimization

The process of combining the aforementioned methods of analysis and optimization techniques is described here. After the Initialization of the GA the 1st generation is evaluated as far as flight performance is concerned. Several designs with different values in the design variables are put through the following process:

1. Tail sizing. If a design fails this step, it is discarded
2. ACC Constraints Check. If a design fails to follow the spatial constraints, its fitness score is penalized (As mentioned in "Constraint Handling" segment)
3. Aerodynamic Analysis. CL(CD) function is calculated with the methods described above.
4. Flight Performance Analysis. Through the application of Energy Maneuverability, sufficient information concerning a design's fitness is known, as it is described by distance, height, calculated by the Routwski – Path and Payload, given by the value of the payload design variable.
5. Evaluated members are put through the Genetic Operators and the same process is applied for new generations until the results converge.

The optimal design is obtained and the reliability of aerodynamic results is tested via CFD validation

4. Results validation via the use of Computational Fluid Dynamics

4.1. Basic Principles of Computational Fluid Mechanics

Achieving the optimal aerodynamic shape has always been a challenge for manufacturers-designers, but nowadays they have an additional powerful tool: computer simulation. The terrifying evolution of computers over the last 30 years has resulted in them becoming a key part of the industrial process. One of the first branches in which the PC was introduced and its importance emerged was Fluid Mechanics. The solution of the complex Navier-Stokes equations, which until then was considered impossible, made it necessary for them to be present in the calculations and simulations in this branch.

In particular, the field of engineering that has developed rapidly in recent years and is the cornerstone of Fluid Engineering is Computational Engineering and Computational Simulation. It is a tool that does not replace experimental tests and test simulation flights, but acts auxiliary and offers speed and low computational cost. It is a dynamically evolving industry that provides answers to a wide range of complex problems using numerical methods such as finite differences and finite volumes.

4.2. Basics of Fluid Engineering

The governing equations of the turbulent flow of a fluid are:

- The continuity equation
- The equation of motion
- The energy equation

4.2.1. Continuity Equation

Applying the principle of conservation of mass to an elementary volume of compressible fluid in a Cartesian coordinate system result in the continuity equation:

$$\frac{\partial \rho}{\partial t} + \frac{\partial(\rho u)}{\partial x} + \frac{\partial(\rho v)}{\partial y} + \frac{\partial(\rho w)}{\partial z} = 0 \quad (1)$$

4.2.2. Momentum Conservation Equation

Applying the principle of conservation of momentum to an elementary volume of compressible fluid, the equations of motion per direction are obtained:

$$\frac{Du}{Dt} = -\frac{1}{\rho} \frac{\partial p}{\partial x} + pf_x + \frac{1}{\rho} \left[\frac{\partial}{\partial x} \left(\mu \frac{\partial u}{\partial x} \right) + \frac{\partial}{\partial y} \left(\mu \frac{\partial u}{\partial y} \right) + \frac{\partial}{\partial z} \left(\mu \frac{\partial u}{\partial z} \right) \right] \quad (2)$$

$$\frac{Dv}{Dt} = -\frac{1}{\rho} \frac{\partial p}{\partial y} + pf_y + \frac{1}{\rho} \left[\frac{\partial}{\partial x} \left(\mu \frac{\partial v}{\partial x} \right) + \frac{\partial}{\partial y} \left(\mu \frac{\partial v}{\partial y} \right) + \frac{\partial}{\partial z} \left(\mu \frac{\partial v}{\partial z} \right) \right] \quad (3)$$

$$\frac{Dw}{Dt} = -\frac{1}{\rho} \frac{\theta p}{\theta z} + p f_z + \frac{1}{\rho} \left[\frac{\theta}{\theta x} \left(\mu \frac{\theta w}{\theta x} \right) + \frac{\theta}{\theta y} \left(\mu \frac{\theta w}{\theta y} \right) + \frac{\theta}{\theta z} \left(\mu \frac{\theta w}{\theta z} \right) \right] \quad (4)$$

4.2.3. Energy Conservation Equation

Applying the principle of conservation of energy to an elementary volume of compressible fluid results in the equation of conservation of energy:

$$\begin{aligned} \frac{\theta}{\theta t} \left[\rho \left(e + \frac{V^2}{2} \right) \right] + \nabla \cdot \left[\rho \left(e + \frac{V^2}{2} \vec{V} \right) \right] &= \rho \dot{q} + \frac{\theta}{\theta x} \left(k \frac{\theta T}{\theta x} \right) + \frac{\theta}{\theta y} \left(k \frac{\theta T}{\theta y} \right) + \\ &+ \frac{\theta}{\theta x} \left(k \frac{\theta T}{\theta z} \right) - \frac{\theta (up)}{\theta x} - \frac{\theta (vp)}{\theta y} - \frac{\theta (wp)}{\theta z} + \frac{\theta (u\tau_{xx})}{\theta x} + \\ &+ \frac{\theta (u\tau_{yx})}{\theta y} + \frac{\theta (u\tau_{zx})}{\theta z} + \frac{\theta (v\tau_{xy})}{\theta x} + \frac{\theta (v\tau_{yy})}{\theta y} + \\ &+ \frac{\theta (v\tau_{zy})}{\theta z} + \frac{\theta (w\tau_{xz})}{\theta x} + \frac{\theta (w\tau_{yz})}{\theta y} + \frac{\theta (w\tau_{zz})}{\theta z} + p \vec{f} \cdot \vec{V} \end{aligned}$$

4.3. Finite Volume Method

Finite volume method is a general method that combines elements of integral methods and difference methods and proves to be particularly efficient in problems involving mass transfer, heat momentum, etc. In this method, the discretization equation used for the numerical solution is obtained by completing differential equations on control volumes. It is one of the most widely used computational methods and is also the basic method used in Ansys Fluent software, the same software we used to perform CFD simulation for our model UAV.

4.3.1. 2-D Finite Volume Method

Consider the general transfer equation which we complete on a volume V which is enclosed by a surface A:

$$\iiint_V \frac{\theta}{\theta t} (\rho \varphi) dV + \iiint_V \operatorname{div} (\rho u \vec{\varphi} - \Gamma_\varphi \operatorname{grad} \varphi) dV = \iiint_V S_\varphi dV$$

And:

$$\frac{\theta}{\theta t} \iiint_V (\rho \varphi) dV + \iiint_V \operatorname{div} (\rho u \vec{\varphi} - \Gamma_\varphi \operatorname{grad} \varphi) dV = \iiint_V S_\varphi dV$$

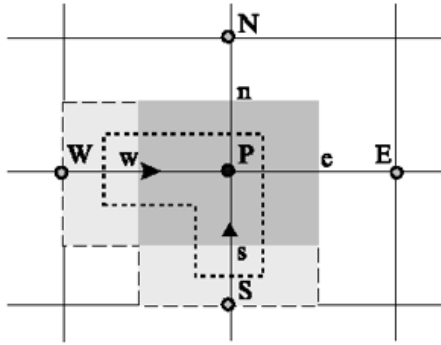
Considering the average values of the quantities in the control volume V we get:

$$\frac{\theta}{\theta t} [\rho \varphi] \Delta V + \iiint_V \operatorname{div} (\rho u \vec{\varphi} - \Gamma_\varphi \operatorname{grad} \varphi) dV = [S_\varphi] \Delta V$$

Applying Gauss' theorem, we convert the spatial integral of the flow rate deviation of the gradient magnitude φ to a surface integral as follows:

$$\frac{\theta}{\theta t} [\rho\phi] \Delta V + \iint_{A} (\rho u \vec{\phi} - \Gamma_{\phi} \text{grad} \phi) \cdot \vec{n} dA = [S_{\phi}] \Delta V$$

The calculation of the spatial integral requires the discretization of the study area into distinct finite volumes of random size but always of Cartesian topology. In each control volume we specify a point at which the values of the graded quantities are stored. In order to create the grid, other such central storage points of scaled sizes are defined. The boundaries of the control volumes are placed in the middle of the distance of the adjacent points-nodes. The values of the non-scaled quantities are stored on the surfaces of the control volumes, always depending on the scaled quantities. This means that triple points (P, w, s) are stored in the same memory location of the computer even though the location of all three points is not identical in the control volume.



4.3.2. FVM Discretization Grid

Eventually three sets of finite volumes emerge: one for gradients, one for u-velocities, and one for v-velocities. The application of the general transfer equation in its integral form on the control volume gives:

$$\frac{d}{dt} [\rho\phi] V_P + g_e - g_w + g_n - g_s = [S_{\phi}] V_P$$

Making the appropriate assumptions the transfer equation is discretized as follows:

$$\frac{\rho_P \phi_P - \rho_P^0 \phi_P^0}{\Delta t} + (CE + DE) - (CW + DW) + (CN + DN) - (CS + DS) = S_{\phi, P} V_P$$

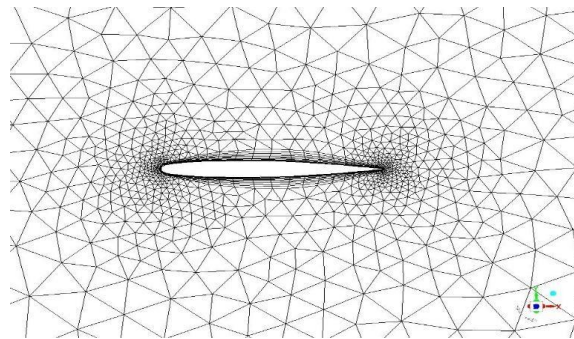
,where:

$$\begin{aligned} CE &= (\rho u)_e A_e \phi_e & DE &= -\Gamma_e A_e \left. \frac{\theta \phi}{\theta x} \right|_e \\ CN &= (\rho u)_w A_w \phi_w & DW &= -\Gamma_w A_w \left. \frac{\theta \phi}{\theta x} \right|_w \\ CS &= (\rho v)_s A_s \phi_s & DS &= -\Gamma_s A_s \left. \frac{\theta \phi}{\theta y} \right|_s \end{aligned}$$

To fully discretize the transfer equation, it is necessary to calculate the values of the variable ϕ and its derivatives at the fronts of the control volumes (n, s, e, w) as a function of the values at points N, S, E, W. There are many methods to do so like upwind scheme or central difference scheme. The extension from the 2-D FVM method to the 3-D is easy.

4.4. Hermes V CFD Simulation

For the best design of our model UAV - HERMES V, our team performed CFD Simulation both on the entire UAV and on each of its free surfaces. The software used for this purpose is BETA's "ANSA" grid creation software as well as Ansys "Fluent" Solver. The finite volume method – FVM is used in the Ansys Fluent Solver. Box-type mesh was created for every simulation we conducted.

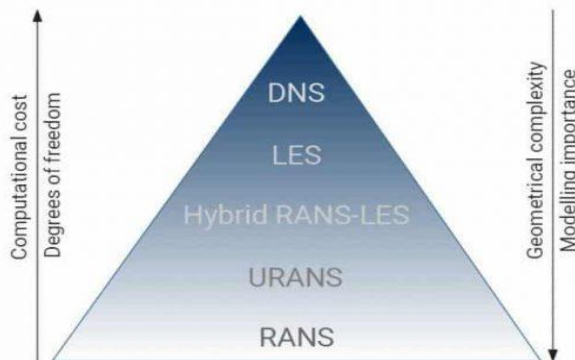


4.4.1. Turbulence Model

A turbulent flow is characterized by fluctuations in the velocity field. These fluctuations mix the quantities that are transferred such as mass and momentum and cause fluctuations in them as well. These variations are computationally too "accurate" to be calculated directly numerically and simulated due to the small scale and high frequencies that occur. For this reason Direct Numerical Simulation (DNS) is not suitable for industrial applications.

To resolve this problem, various approaches have been formulated based on some assumptions in order to make the calculation possible within acceptable time and computational limits:

- RANS models (Reynolds - Averaged Navier - Stokes)
- Model LES (Large Eddy Simulation)



4.4.2. RANS Turbulence Models

In this approach we accept that the instantaneous velocity value is the sum of time average and fluctuation term:

$$u_i = \overline{u_i} + u_i'$$

Similarly for pressure and other gradients we get:

$$\varphi_i = \overline{\varphi_i} + \varphi_i'$$

Substituting expressions of this form into the momentum and continuity calculation equations and taking the time average we get:

- $\frac{\theta \rho}{\theta t} + \frac{\theta}{\theta x_i} (\rho u_i) = 0$
- $\frac{\theta}{\theta t} (\rho u_i) + \frac{\theta}{\theta x_j} (\rho u_i u_j) = -\frac{\theta p}{\theta x_i} + \frac{\theta}{\theta x_j} \left[\mu \left(\frac{\theta u_i}{\theta x_i} + \frac{\theta u_j}{\theta x_i} - \frac{2}{3} \delta_{ij} \frac{\theta u_k}{\theta x_k} \right) \right] + \frac{\theta}{\theta x_j} (-\overline{\rho u_i' u_j'})$

These two equations are the RANS (Reynolds-Averaged Navier-Stokes) equations. We observe, however, that in the last equation additional terms appear which represent the effect of turbulence. These new unknowns are hidden in the terms: $-\overline{\rho u_i' u_j'}$ which are the terms of the Reynolds trends. In other words, we have a system of 4 equations and 7 unknowns which we have to model in order to deal with the closure problem.

4.4.3. Boussinesq Case

The modeling of Reynolds trends is based on Boussinesq's hypothesis that Reynolds stresses are related to time slopes:

$$-\overline{\rho u_i' u_j'} = \mu_t \left(\frac{\theta u_i}{\theta x_j} + \frac{\theta u_j}{\theta x_i} \right) - \frac{2}{3} \left(\rho \kappa + \mu_t \frac{\theta u_k}{\theta x_k} \right) \delta_{ij}$$

The Boussinesq hypothesis is used in the Spalart-Allmaras model, k-ε models and k-ω models. The advantage of this approach is the relatively low computational cost.

4.4.4. Spalart-Allmaras Turbulence Model

This one-equation model, is the turbulence model that we used in our simulations as it is preferred for aerodynamic applications in external flows and is described by the following equation:

$$\frac{\tilde{\theta} v}{\theta t} + v_j \frac{\tilde{\theta} v}{\theta x_j} = c_{b1} (1 - f_{t2}) \tilde{S} v - \left[c_{w1} f_w - \frac{c_{b1}}{k^2} f_{t2} \right] \left(\frac{v}{d} \right)^2 + \frac{1}{\sigma} \left[\frac{\theta}{\theta x_j} \left((v + \tilde{v}) \frac{\tilde{\theta} v}{\theta x_j} \right) + c_{b2} \frac{\tilde{\theta} v}{\theta x_i} \frac{\tilde{\theta} v}{\theta x_j} \right]$$

where:

$$\mu_t = \tilde{\rho} \nu f_{v1}$$

$$f_{v1} = \frac{\chi^3}{\chi^2 + c_{v1}^3}, \quad \chi = \frac{\tilde{\nu}}{\nu}, \quad \mathbb{S} = \Omega + \frac{\tilde{\nu}}{k^2 d^2} f_{v2}, \quad \Omega = \sqrt{2W_{ij}W_{ij}}, \quad W_{ij} = \frac{1}{2} \left(\frac{\theta u_i}{\theta x_j} - \frac{\theta u_j}{\theta x_i} \right),$$

$$f_{v2} = 1 - \frac{\chi}{1 + \chi f_{v1}}, \quad f_w = g \left[\frac{1 + c_{w3}^6}{g^6 + c_{w3}^6} \right]^{1/6}, \quad g = r + c_{w2}(r^6 - r), \quad r = \min \left[\frac{\tilde{\nu}}{\mathbb{S} k^2 d^2}, 10 \right],$$

$$f_{t2} = c_{t3} \exp(-c_{t4} \chi^2)$$

and for the constants:

$$c_{b1} = 0.1355, \quad c_{b2} = 0.622, \quad \sigma = 2/3, \quad \kappa = 0.41, \quad c_{w2} = 0.3,$$

$$c_{w3} = 2, \quad c_{u1} = 7.1, \quad c_{t3} = 1.2, \quad c_{t4} = 0.5, \quad c_{w1} = \frac{c_{b1}}{k^2} + \frac{1 + c_{b2}}{\sigma}$$

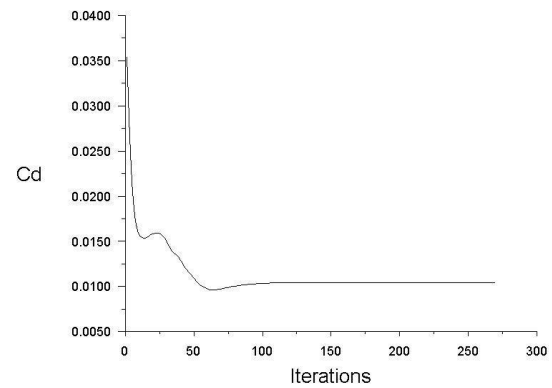
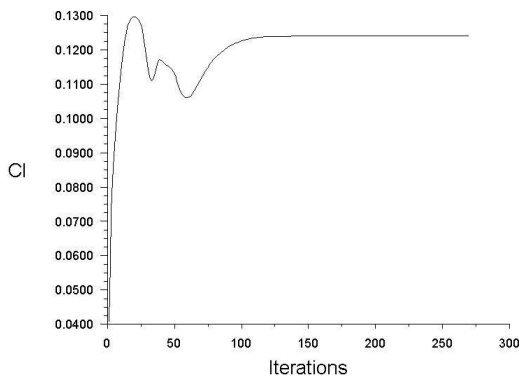
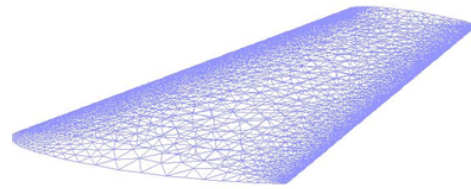
After the meshing and the turbulence model choice we determined the:

- Materials: air as the fluid and aluminum as the solid with their properties
- Operating conditions: determined for pressure, density, gravity and temperature
- Inlet and outlet conditions: based on our mission instructions
- Wall conditions: standard wall function was used for near wall treatment
- Reference values: computed from initial conditions
- Solving preferences:
 1. Coupled scheme between pressure and velocity
 2. Second Order Upwind Scheme for pressure, density, momentum and energy
 3. First Order Upwind Scheme for modified turbulent viscosity

We also used a pseudo-transient option as well as high order term relaxation with value of 0.75.

- The initial values for the simulations were computed from the inlet conditions

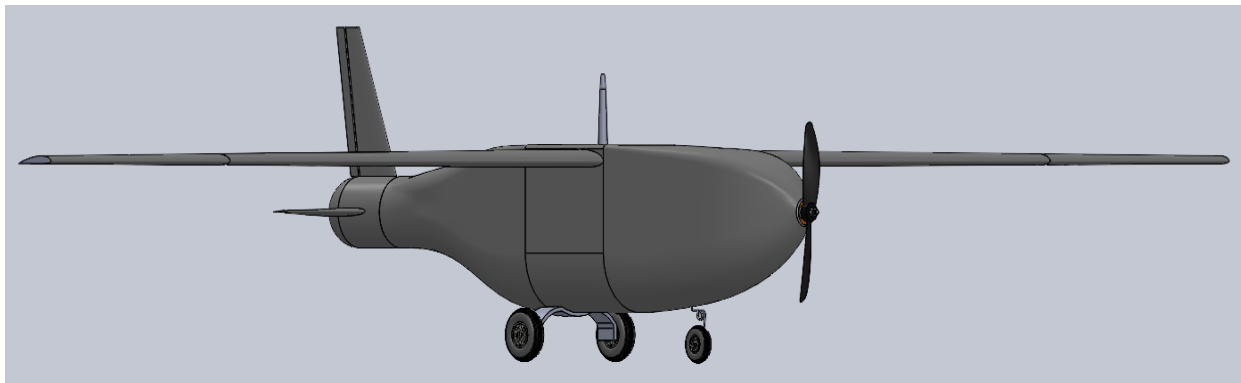
The results from the CFD simulation were compared to the results from the VOGEL program and used to validate our initial assumptions.



5. Structural design

5.1 Model Design

Designing the aircraft's fuselage was a multifactorial process on which the structural team worked for several months. Initially the main objectives were the ones given by the competition while also using the least resources necessary, however it was later required to meet the constraints computed from the aerodynamic analysis. Given the aforementioned, the resulting geometry is the one depicted in the picture below, which will be analyzed later on.



The front of the aircraft has a cylindrical profile in order to fit the given motor. Moving towards the cargo bay, the plane's profile changes to a U shaped one, necessary to fit the required cargo without using unnecessary material. The cargo bay has a total length of 170 [mm] and a thickness of 3 [mm] and is designed to hold both the blood bags and the battery. These components are not secured on the fuselage itself, but are rather placed in a tray able to move slightly (approximately ± 3 [cm]) along the fuselage's axis. The latter was considered a convenient way to shift the aircraft's center of mass to the optimal position for each flight. Moving past the cargo bay, the fuselage becomes both smaller and thinner, so that flow separation does not occur, while at the same time having sufficient pressure at the elevator wing's suction side. The back of the aircraft is also of cylindrical geometry, and fits the servo mechanisms needed to rotate the elevator wings and the rudder wing's moving component. It has an inner radius of 460 [mm] and a thickness of 2 [mm]. The transition between different geometries is achieved using proper spline curves. The telemetry is placed at the top of the plane's cargo bay.

Given that the motor is of cylindrical shape and has a diameter of 35 [mm], such is the geometry of the very front of the fuselage, with a tolerance of 1 [mm]. The base on which the motor is secured is rather simple, being a rectangular shape with the necessary holes for the screws. It is placed internally, so that only the front of the motor with the propeller protrudes out of the plane's body.

The cargo bay's tray is one of the most crucial components of the design, since it is used both to properly secure the cargo and to shift the model's center of mass. In correspondence with the above, particular attention was given to designing it. It is of a parallelepiped shape, with dimensions of 108x148x170 [mm] (X x Y x Z). The 8 [mm] tolerance on the x – axis is filled with a sponge-like material, to secure the blood bags in place. On the lower side, the tray has a T – shaped edge to be placed appropriately to a similar shaped rail attached to the fuselage's belly. That way, movement is constrained in the Y and X axis, but is allowed in the Z axis. Once the tray is placed at the desired position, it is secured using a screw with a screw and rubber. The screw is used to define the tray's position, and the rubber friction ensures the latter will not be unscrewed.

The part of the fuselage between the cargo bay and the back of the plane has no practical implementation other than achieving the desired body length, and only contains cables ending up to the elevator and rudder servo mechanisms. The latter are secured with screws in properly designed bases attached to the lower inner surface of the body.

The elevator wings are connected with a beam with a rectangular shape in the middle of it, on which the servo mechanism attaches. This way, more torque is produced to rotate the wings to

the desired degrees. The rudder wing's moving component is attached to the stable one with a hinge.

Finally, the wing had to be split into two distinct components in order to fit the competition's spatial constraints (wooden box). The two parts are connected to each other with two circular beams. Similarly, the two main wings are connected with two larger beams that go through the upper part of the fuselage.

The model was designed using SOLIDWORKS and Fusion360 softwares.

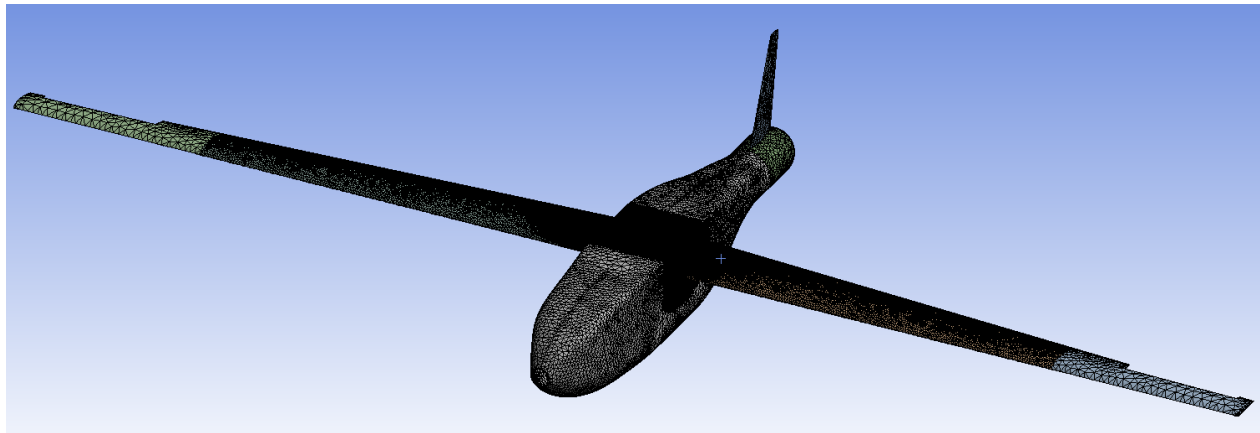
5.2. Structural analysis

For the purposes of modeling the stresses the airplane will be required to withstand during the static test, it was decided to perform a simulation of static stress. The case was simulated in ANSYS' Mechanical APDL while the mesh was also created with ANSYS' mesher. The materials used were Structural Steel and PLA, the main idea being if the model can withstand its own weight, it will certainly do so when coated with carbon fiber. More specifically, structural steel was applied to the beam placed at the wings' interiors, while the rest of the material was set to be PLA. Since the material library does not contain PLA, it had to be constructed as a new material with the physical properties depicted below.

	A	B	C
1	Property	Value	Unit
2	 Density	1250	kg m ⁻³
3	 Isotropic Secant Coefficient of Thermal Expansion		
4	 Coefficient of Thermal Expansion	0.000135	C ⁻¹
5	 Isotropic Elasticity		
6	Derive from	Young's Modulus an...	
7	Young's Modulus	3.45E+09	Pa
8	Poisson's Ratio	0.39	
9	Bulk Modulus	5.2273E+09	Pa
10	Shear Modulus	1.241E+09	Pa
11	 Tensile Yield Strength	5.41E+07	Pa
12	 Tensile Ultimate Strength	5.92E+07	Pa
13	 Isotropic Thermal Conductivity	0.144	J m ⁻¹ s ⁻¹ C ⁻¹
14	 Specific Heat, C _p	1190	J kg ⁻¹ C ⁻¹
15	 Isotropic Resistivity	4.31E+09	ohm m

5.2.1 Mesh

Concerning the model's mesh, linear elements were used with their size set to 10 [mm]. A sphere of influence was defined at the upper side of the cargo bay area, with a radius of 150 [mm] and an element size of 2.5 [mm]. The sphere influenced both the surfaces of the fuselage and the wings. Last but not least, the element size on the upper sides of the wings was set to be 5 [mm]. The mesh's final statistics turned out to be 357.448 nodes and 184.853 elements.

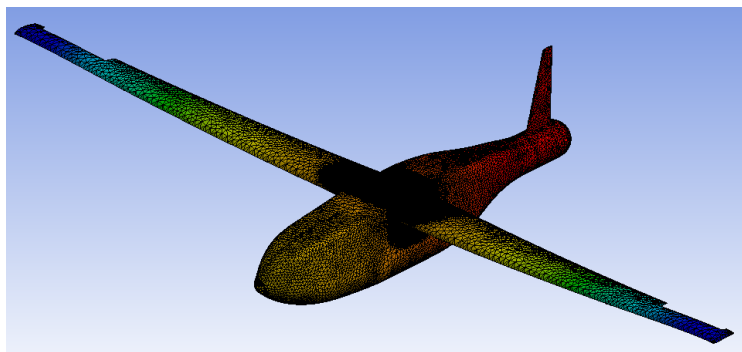


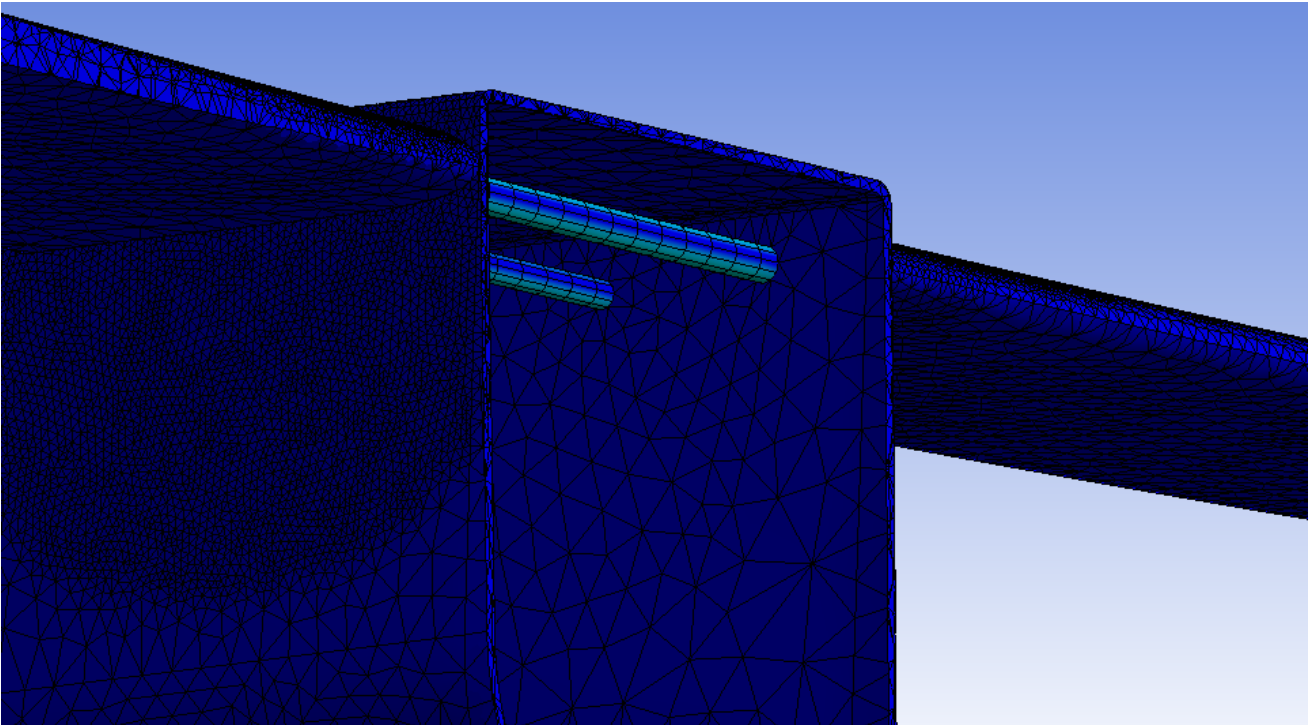
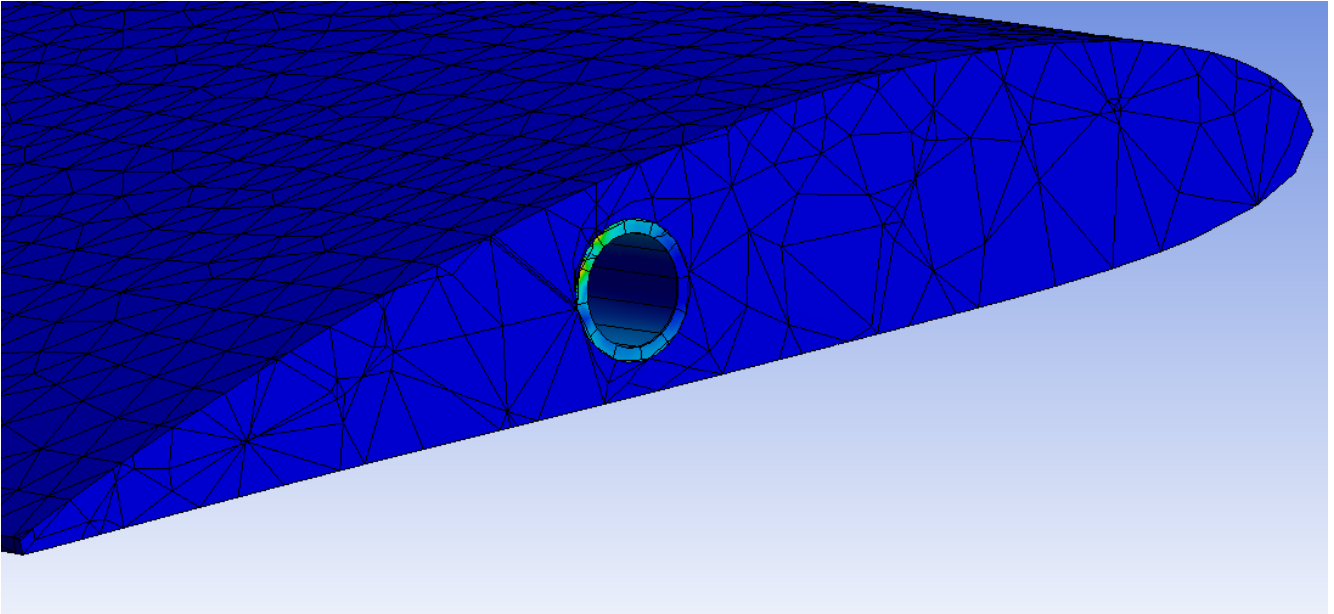
5.2.2. Case Setup

Regarding the loads and constraints, the surfaces at the tips of the wings were defined as fixed. Earth gravity was toggled on and the weights of the components not included in the CAD design were modeled as distributed forces applied at the corresponding positions.

5.2.3. Simulation

The total deformation was more severe at the back of the plane, as depicted below, with a maximum of 66.096 [mm] at the rudder wing. Concerning the equivalent (von-Mises) stress, the maximum appeared to be applied at the circular beams connecting the beams with the fuselage of the aircraft, with a value of 247.389 [MPa]. Given that the previously mentioned results were within the acceptable margins of the used materials, the final design coated with carbon fiber is sure to withstand the loads applied in this simulation.





6. Payload prediction

As discussed in the previous sections, a full body design optimization approach was used. Crucial in the performance assessment of each design is the Weight Prediction and thus the available operational Payload.

Payload is one the competition's objectives and is included in the scoring function and thus was one of the design variables to be optimized. The model for the weight prediction was based on empirical estimation of component weight as a function of the specific weight for the material used for a unit of surface. The generic formula is:

$$W_{component} = w_s (kg/m^2) * S(m^2)$$

The final Weight formula is as follows:

$$W_{Take-off} = \Sigma[W_{fixed}] + \Sigma[W_{component}] + W_{payload}$$

For every generated design in the Genetic Algorithm, this methodology was implemented to estimate the initial Take-Off weight. Adding the component weight estimation with the payload prediction we acquire the estimated Take-off Weight. This weight is used throughout the mission performance analysis. The payload prediction is an independent design variable generated in the beginning of the performance analysis and is later added in the analysis. This approach includes the possibility of a payload prediction that is finally not acceptable by the performance of the corresponding airframe design. In this case, this design is rejected totally and follows the procedure mentioned in the "Constraint Handling " section. If the predicted payload is operationally acceptable then this value is used for the later handling by the Genetic Algorithm.

In the case of our selected final design, a payload value of

$$W_{payload} = 0.92 \text{ kg}$$

was estimated and found suitable for the performance of the corresponding design.

7. Manufacturing

The airplane construction was broken up into three individual parts: fuselage, wing, and empennage. All the parts were designed with the ability to be taken apart for shipping and storage purposes and then assembled together. There were many things to consider in the manufacturing plan, including the material selection and construction methods.

7.1 Material Selection

The criteria for the materials included: strength, weight, ease of manufacturing, and cost. After completing research on modern materials suitable for use in model airplanes, it was found that the most common are balsa wood, plastic, alloys such aluminum, and composites such as carbon

and fiberglass. All of these materials have specific attributes that make them suitable for specific applications, and these attributes had to be taken into consideration to make a decision.

Balsa wood is found in most model aircraft today due to its inexpensive cost and large availability. Balsa wood is a very low-density material that is frequently used to build the structural frame of the fuselage and wing. Unlike metals and some composites, balsa wood is relatively easy to shape as desired. It is also very strong in tension, but does not perform as well in compression. When utilized by itself to build an aircraft structure, it needs to be built with a truss system for structural support, which is often time intensive.

Plastic is used primarily for small components such as fasteners and control systems in model aircraft. It can be used for both internal and external airplane structures, but since it has a high density and manufacturing processes involving it are complicated, plastic is not a desired material of choice. On the other hand, 3d-printing technology allows us to reduce the weight of a plastic construction in acceptable scale. In this way we could take into consideration the usage of plastic for the construction of the fuselage and the wing.

Alloys are mainly utilized for structures on larger models and full-scale aircraft. An alloy, such as aluminum, contains properties that allow it to be very light yet extremely strong in both torsion and bending. This material can be best utilized in high stress areas such as the wing spar and tail beam. However, alloys such as aluminum still have a relatively high density compared to non-metals, and if the emphasis is on weight reduction, a high grade of alloy must be used. This requirement makes aluminum parts very expensive. Metals require specific tools to machine, which makes it difficult to quickly change design or repair a damaged part.

Composite materials require time consuming planning and processes, yet can allow for considerable weight savings without compromising strength and safety. Composite materials are typically strong in one specific direction thus requiring additional analysis of the structure to plan for compensating the stress that develops in the direction counter to the composite's strengths. These materials are typically strongest in the direction that the fiber strands are in tension. For this reason, composites are set up in layers and then a very strong resin is applied to bond the layers together. The most common types of composites are fiberglass and carbon fiber. The difference between the two types is in strength and weight. Carbon fiber can hold up to far more stresses than fiberglass. It is very important that no metal should touch the carbon fiber material so as to prevent radio interference.

7.2 Manufacturing Process

The carbon fiber cloth (without epoxy) will be laid into a mold of each part required for building. The layers being placed will have specific orientation, which will be determined by analyzing the structure. Once the layers have been placed into the mold, the epoxy will be added, and the

entire part will be vacuum bagged to rid the epoxy and fabric of any excess air which could weaken the material. Once the epoxy has set, the part can be sanded and is then ready for flight.

There are two different types of manufacturing processes that were used. The different types were referred to as Type A and Type B construction methods. Type A construction method was used to make shell components such as the fuselage and wing skins. Type B construction method was used to make the internal structure of the airplane that included support parts and ribs.

7.2.1 Type A Construction Process

In the Type A construction process, the shape of the airplane components was created by 3d-printing technology, from PLA material. These PLA parts, referred to as “masters”, were used to make the plaster molds as shown in Figure 5.2.1. Only the “shell” components of the airplane structure (like wing, fuselage, beams etc.) needed these masters to form the shape of the mold. The molds were used to lay the carbon fiber cloth, which in turn will be soaked in a Polyvinyl Ester resin and left to cure in a vacuum bag system for 24 hours.

The clam-shell technique was used for assembling the shells. The top and bottom sides of the wing were made separately and were glued together in the final assembly. The seams were filled and sanded to ensure a smooth surface.

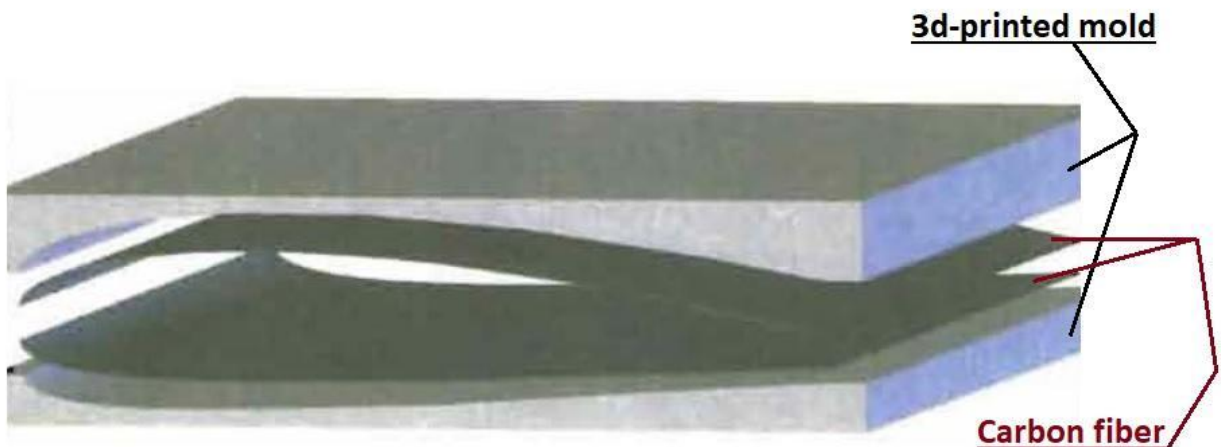


Figure 5.2.1

7.2.2 Type B Construction Process

The Type B construction process was used to make the support parts and ribs as shown in Figure 5.2.2 and 5.2.3. This process belongs to the 3d-printing technology sector and the technique that was chosen is the “Fused Filament Fabrication”.

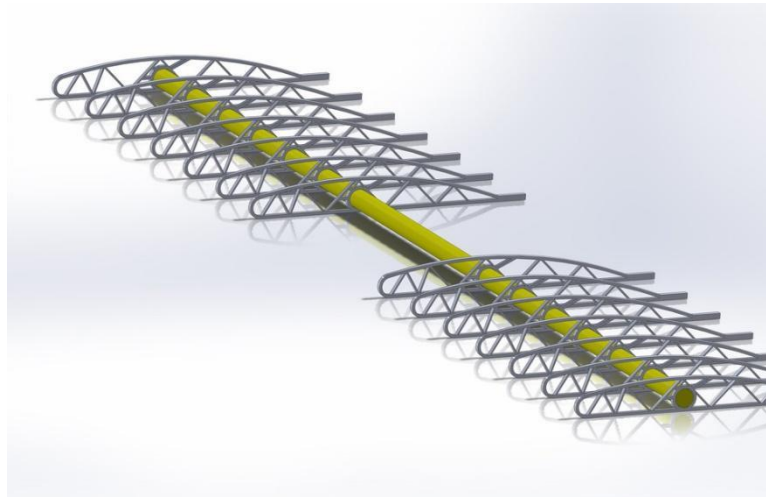


Figure 5.2.2

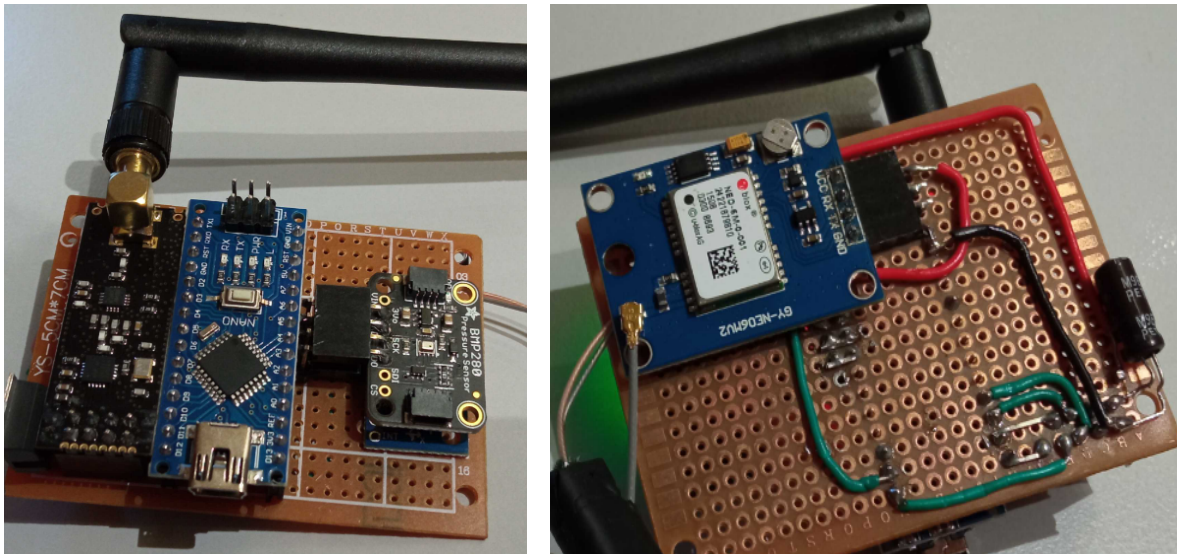


Figure 5.2.3

8. Telemetry Development

A highly important aspect of our aircraft's development depends on its flight data analysis. On that note, last year our electrical team designed and developed a telemetry system with ground to air communication. Having such a system is essential, as we use it not only to have a live and detailed image of our aircraft's behavior under various weather conditions but also as a means for our pilot to train, allowing him to acquire consistency and precision when flying the aircraft. Our telemetry system's development began a year ago and was used to gather data such as altitude, location and flight characteristics. This year, the team's main focus was the improvement of our existing telemetry in terms of software and hardware so it harmonically fits our new aircraft's needs. The key points of the telemetry system's design were, firstly, choosing high quality hardware parts, in order to achieve precision, but at the same time keeping them low-budget and thus, easily replaceable. Secondly, we used open-source software which allowed us to have a highly customizable interface for the data analysis and visualization and also aligned with our low-budget philosophy. After reaching the desired point of its development the telemetry system was installed on the aircraft and was used during test flights with greatly sufficient results.

Under a more technical scope, the hardware we used was an Arduino Nano equipped with an accelerometer (MPU6050), a barometer (BMP280), a GPS (UBLOX NEO 6M), a transmitter (nRF24L01) and a power module which provides 5 Volts to the whole system.



All these sensors collect many and different readings that provide us with the data mentioned above. More specifically, these readings are the battery voltage of the system to ensure its reliability, the GPS coordinates (longitude and latitude) as well as the altitude and ground speed provided from the GPS module. In addition, we have measurements about the accelerations and

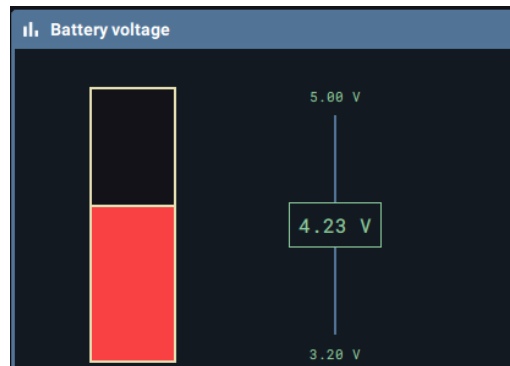
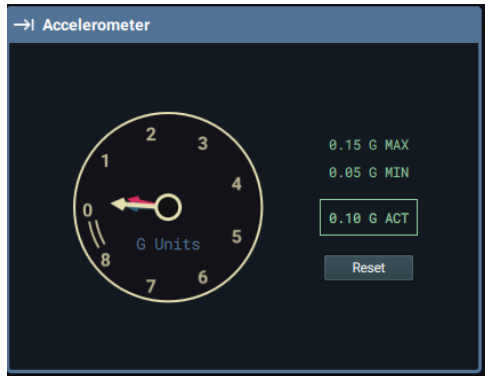
angles in all axes, the altitude provided from the barometer which is more reliable and accurate and finally the temperature. This useful information is easier to interpret in visual form. With that in mind we used Serial Studio as an open-source program to visualize the data in a way that the pilot could easily understand and make corrections in real time. Below we present the board, graphs and widgets used for each of the measurements we mentioned.

Mission Status		Sensor Readings		GPS		Accelerometer	
Runtime	16987 [ms]	Temperature	27.85 [°C]	Longitude	23.9232254 [°E]	X	0 [m/s ²]
Battery voltage	4.27 [V]	Altitude	113.28 [m]	Latitude	37.8842163 [°N]	Y	-0.14 [m/s ²]
		speed - air	0 [kph]	Altitude	112 [m]	Z	1 [m/s ²]
				Speed - ground	0 [kph]		

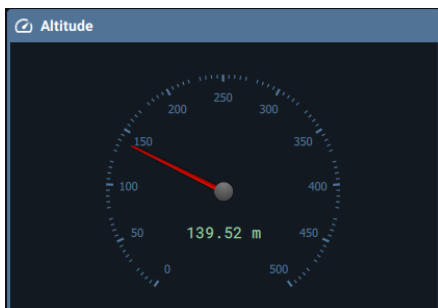
For the GPS position and altitude:



For the accelerations and battery voltage:



For the altitude and ground speed:



9. Outlook

With this year's mission coming to an end, it is important that we highlight all the valuable knowledge and experience our team gathered throughout this time. With regards to technical knowledge no one can deny the vital importance of hands-on experience on realistic tasks. On that note, being a part of the Hermes team and taking part in ACC competition offered countless opportunities for all our team members.

For our senior members this competition proved to be a perfect opportunity for them to apply and test all the theoretical knowledge, accumulated from their studies, into a realistic case-study scenario. Through all the design meetings they put to work many of the skills developed by their experience as engineering students. When these would not suffice they enriched their knowledge by researching standard and state of the art methods as defined by academia and industry. Having to come up with answers to a hands-on task, while taking into account various parameters, wasn't an easy process and it definitely provided valuable experience which will no-doubt prove to be valuable in their future careers.

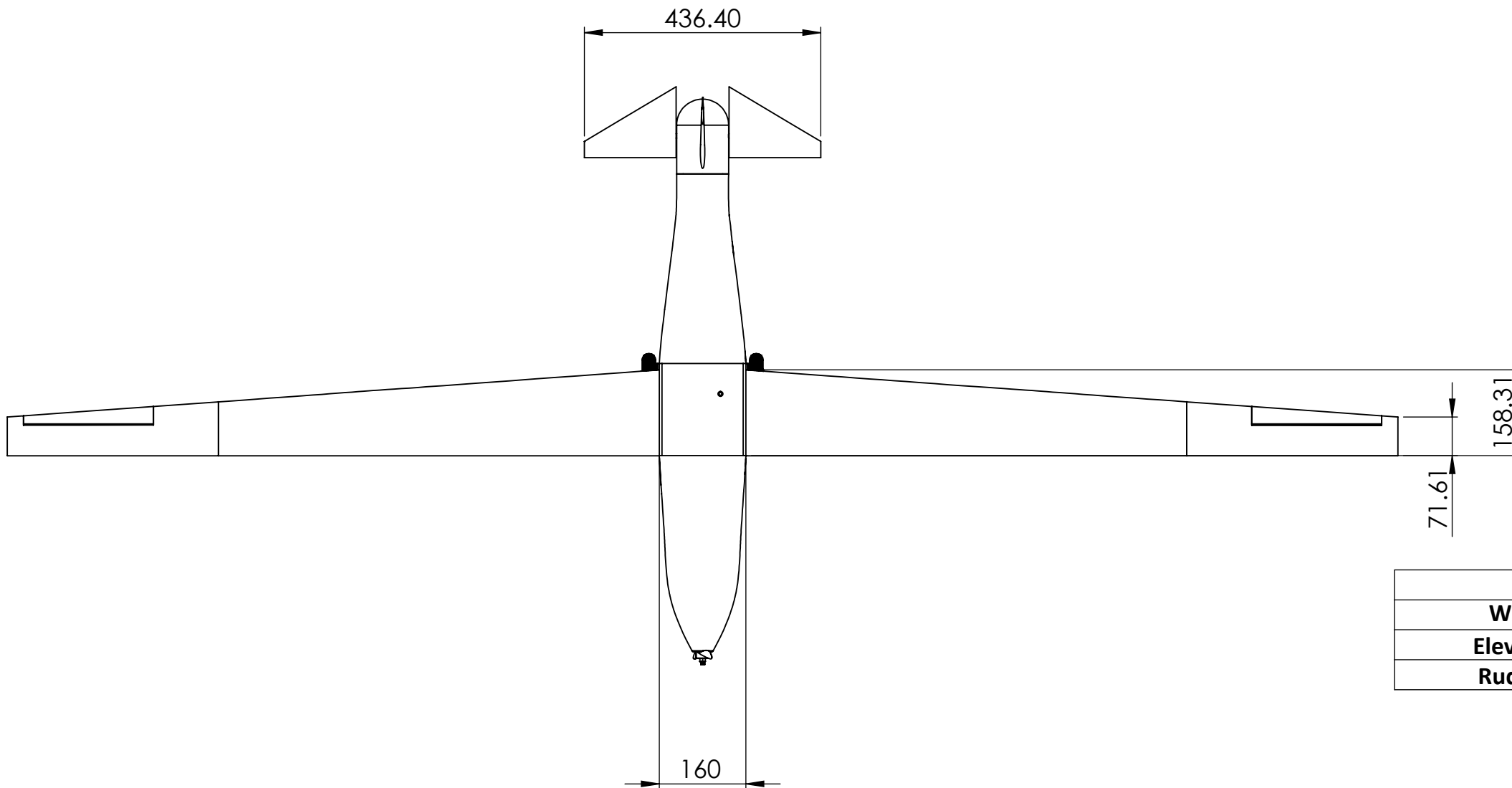
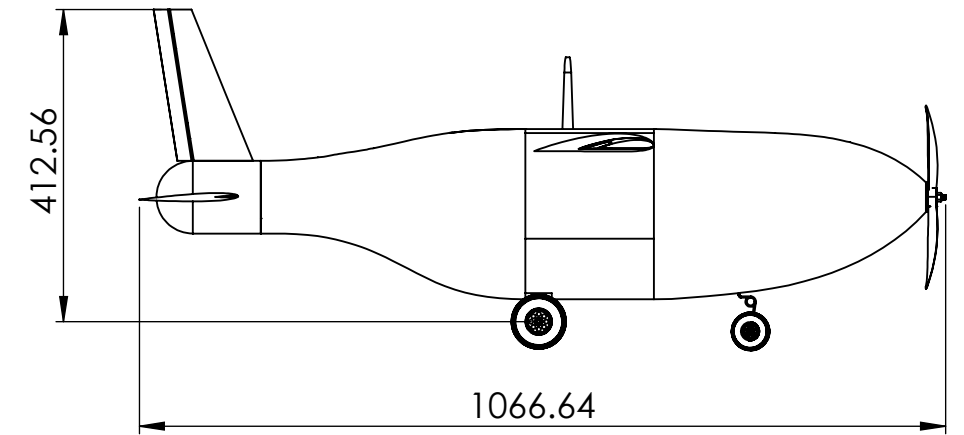
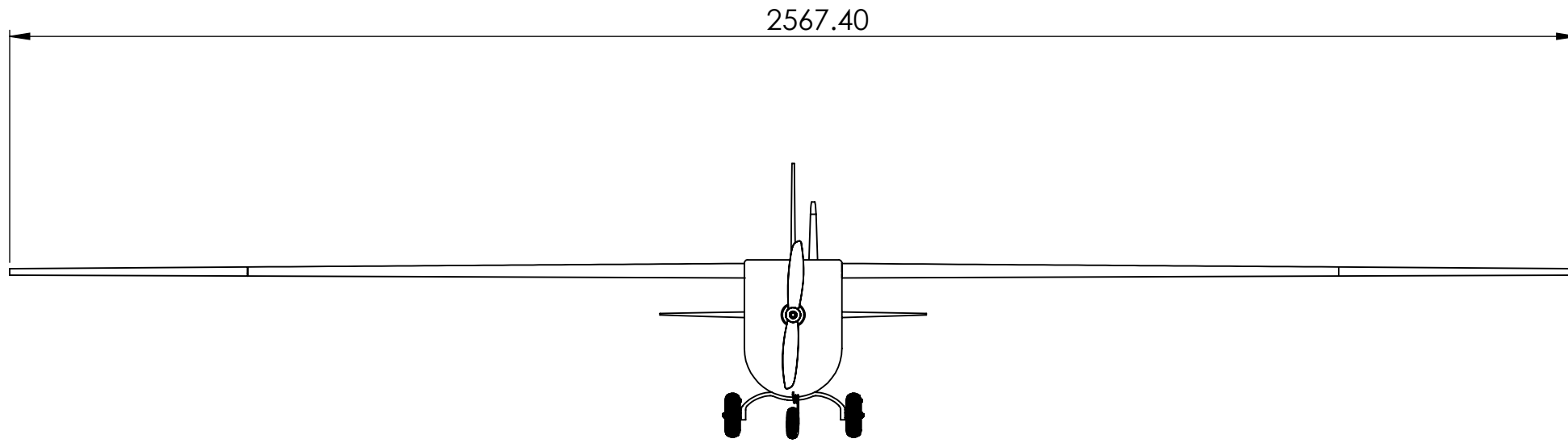
For the members of our team still in their early years of their studies, being a part of the Hermes team gave them insight and inspiration for their studies. It, also, provided an environment for them to closely see how engineers work, how a team is organized and how a task is divided and shared within team members in order to be tackled. Being part of the process of developing our team's aircraft and participating wherever possible, but also, watching the older team members working was an amazing and greatly educational experience.

As a team, the current competition gave us a chance to reorganize and reorient ourselves. With our global optimization approach we developed modular software, with the goal of it being ever and ever improved. We managed to develop tools that we deem vital for an optimization study of any aircraft and may be expanded upon and transformed in the future of our team. Regarding manufacturing, tackling the process with as few outside parties and contractors as possible provided us the experience and tools required to manufacture high performance 3d printed and carbon parts.

Of course, the process was not unhindered and the team came together several times to review the strategy towards the design process and discuss the various aspects that could possibly have been neglected. Moreover, there were many occasions that the process was behind the working schedule and we had to adjust the working speed and delegate work to more people. Construction proved to be much more challenging than expected and we experienced many failed tries, resulting in loss of time and resources.

To sum up, taking part in this year's ACC, we are confident that we have worked hard and in an efficient way and that our effort will be reflected in our team's performance. Of course we wouldn't be here if it weren't for those who helped us along the way. This includes our sponsors, the university faculty, our overseeing professor Dr. S. Voutsinas, and all of the core members of EUROAVIA Athens.

10. Drawings



	Used airfoil	Area(m ²)
Wing	NACA 4415	0.29
Elevator	NACA 0008	0.03
Rudder	NACA 0008	0.03



National Technical
University of Athens

Air cargo challenge
2022

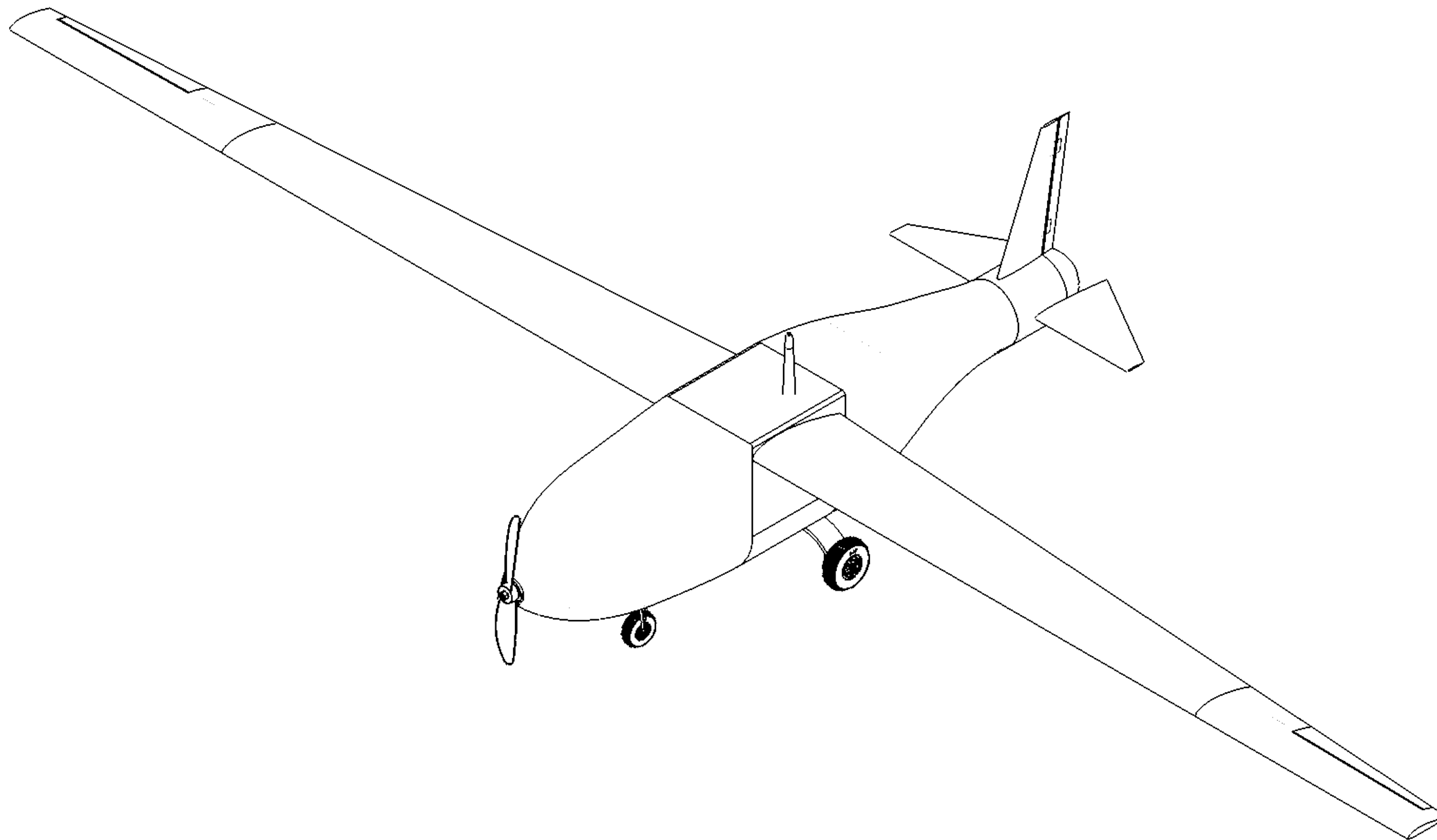
EUROAVIA Athens HERMES Team

HERMES V
3-view drawing

01/05/2022

Scale
1:15

Sheet
1 / 4



National Technical
University of Athens

Air cargo challenge
2022

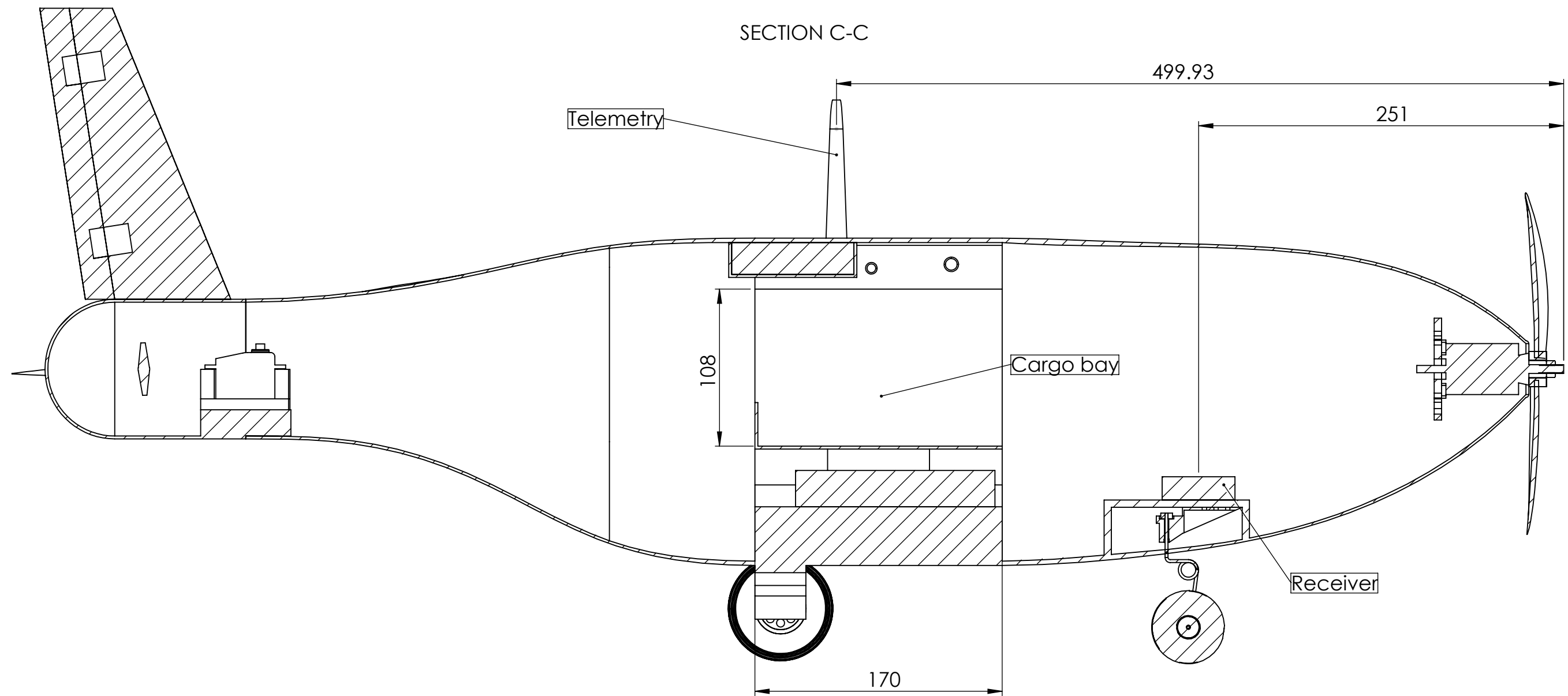
EUROAVIA Athens HERMES Team

HERMES V
Isometric

01/05/2022

Scale
1:6

Sheet
2 / 4



National Technical
University of Athens

Air cargo challenge
2022

EUROAVIA Athens HERMES Team

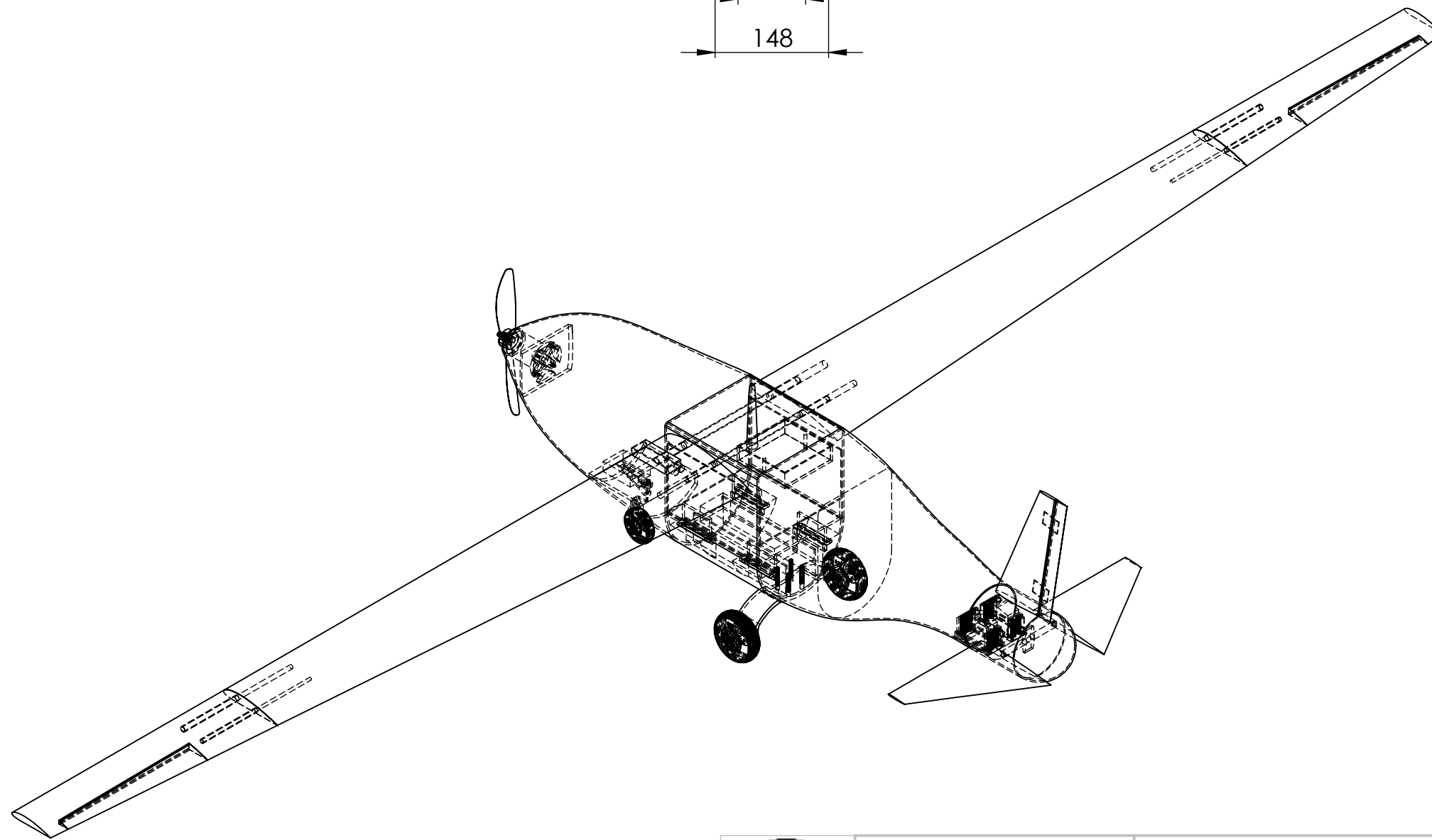
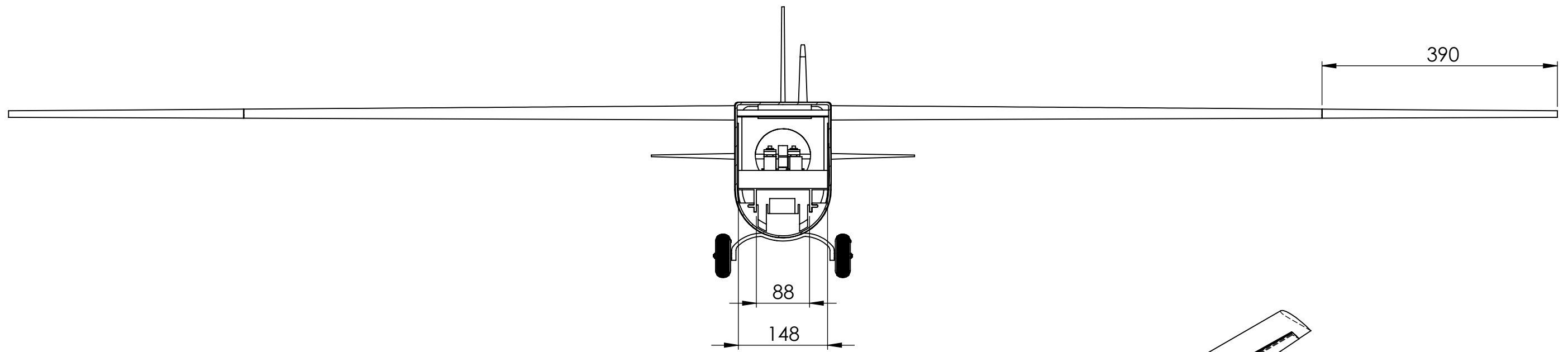
HERMES V
Section View

01/05/2022

Scale
1:3

Sheet
3 / 4

SECTION G-G



National Technical
University of Athens

Air cargo challenge
2022

EUROAVIA Athens HERMES Team

HERMES V
Cargo bay section view

01/05/2022

Scale
1:7

Sheet
4 / 4